

Unchanged top surface-state structures in three-dimensional topological insulator Sb_2Te_3 thin films in the presence of bottom-surface moiré potentials

Dezhi Song(宋德志), Fuyang Huang(黄扶旸), Jun Zhang(仉君), and Ye-Ping Jiang(蒋烨平)
Citation: Chin. Phys. B, 2025, 34 (**12**): 126801. DOI: 10.1088/1674-1056/ae0926
http://cpb.iphy.ac.cn; http://iopscience.iop.org/cpb

What follows is a list of articles you may be interested in

Epitaxial growth of Bi nanowires on Pb-√7 × √3 surface

Siyu Huo(霍思宇), Jieying Li(李洁莹), Yuzhou Liu(刘宇舟), Desheng Cai(蔡德胜), Yitong Gu(谷易通), Haoen Chi(迟浩恩), Wenhui Pang(庞文慧), Gan Yu(于淦), Xiaoying Shi(史晓影), Wenguang Zhu(朱文光), and Shengyong Qin(秦胜勇)
Chin. Phys. B, 2025, 34 (**10**): 106801. DOI: 10.1088/1674-1056/addeb9

Growth and characterization of Bi(110)/$CrTe_2$ heterostructures: Exploring interplay between magnetism and topology

Zhenyu Yuan(袁震宇), Fazhi Yang(杨发枝), Baiqing Lv(吕佰晴), Yaobo Huang(黄耀波), Tian Qian(钱天), Jinpeng Xu(徐金朋), and Hong Ding(丁洪)
Chin. Phys. B, 2024, 33 (**2**): 026802. DOI: 10.1088/1674-1056/ad082a

Molecular beam epitaxy growth of monolayer hexagonal $MnTe_2$ on Si(111) substrate

S Lu(卢帅), K Peng(彭坤), P D Wang(王鹏栋), A X Chen(陈爱喜), W Ren(任伟), X W Fang(方鑫伟), Y Wu(伍莹), Z Y Li(李治云), H F Li(李慧芳), F Y Cheng(程飞宇), K L Xiong(熊康林), J Y Yang(杨继勇), J Z Wang(王俊忠), S A Ding(丁孙安), Y P Jiang(蒋烨平), L Wang(王利), Q Li(李青), F S Li(李坊森), and L F Chi(迟力峰)
Chin. Phys. B, 2021, 30 (**12**): 126804. DOI: 10.1088/1674-1056/ac2e63

Realization of semiconducting Cu_2Se by direct selenization of Cu(111)

Yumu Yang(杨雨沐), Qilong Wu(吴奇龙), Jiaqi Deng(邓嘉琦), Jing Wang(王静), Yu Xia(夏雨), Xiaoshuai Fu(富晓帅), Qiwei Tian(田麒玮), Li Zhang(张力), Long-Jing Yin(殷隆晶), Yuan Tian(田园), Sheng-Yi Xie(谢声意), Lijie Zhang(张利杰), and Zhihui Qin(秦志辉)
Chin. Phys. B, 2021, 30 (**11**): 116802. DOI: 10.1088/1674-1056/ac0037

NBN-doped nanographene embedded with five- and seven-membered rings on Au(111) surface

Huan Yang(杨欢), Yun Cao(曹云), Yixuan Gao(高艺璇), Yubin Fu(付钰彬), Li Huang(黄立), Junzhi Liu(刘俊治), Xinliang Feng(冯新亮), Shixuan Du(杜世萱), and Hong-Jun Gao(高鸿钧)
Chin. Phys. B, 2021, 30 (**5**): 056802. DOI: 10.1088/1674-1056/abeede

---

RAPID COMMUNICATION

Unchanged top surface-state structures in three-dimensional topological insulator Sb_2Te_3 thin films in the presence of bottom-surface moiré potentials

Dezhi Song(宋德志)[†], Fuyang Huang(黄扶旸)[†], Jun Zhang(仉君)[‡], and Ye-Ping Jiang(蒋烨平)[§]

Key Laboratory of Polar Materials and Devices, East China Normal University, Shanghai 200241, *China*

(Received 16 August 2025; revised manuscript received 7 September 2025; accepted manuscript online 19 September 2025)

The exertion of a long-period potential on two-dimensional (2D) systems leads to band-structure downfolding and the formation of mini flat bands, thereby providing a route for band engineering and enabling the realization of new physical phenomena through the tuning of electron–electron interactions. In this work, the effect of the moiré superlattice formed between the substrate and the bottom quintuple layer (QL) of 3- and 4-QL three-dimensional (3D) topological insulator Sb_2Te_3 thin films on the top surface states is investigated. The scanning tunneling spectra reveal that the bulk-like bands exhibit potential variations consistent with the moiré pattern. In contrast, the surface states display only minimal potential variations, resulting in the absence of mini-band formation in the top surface states. These surface states remain nearly unaffected, as confirmed by Landau-level spectroscopy and simulations. The results suggest distinct roles of the bottom-surface moiré potential on the bulk states and the top surface states in the weak coupling regime between the two surfaces.

Keywords: scanning tunneling spectroscopy, topological surface states, heterostructure, moiré potential

PACS: 68.37.–d, 68.37.Ef, 73.20.At, 73.21.Cd

DOI: 10.1088/1674-1056/ae0926 **CSTR:** 32038.14.CPB.ae0926

1. Introduction

When subjected to a long-period 2D potential, the original bands of a 2D system undergo downfolding, and mini flat bands may emerge. The formation of flat bands significantly enhances electron–electron interactions, giving rise to phenomena that may be unattainable in the pristine state of the material.[1–7] In 3D topological insulators (TIs), the mini bands formed from the 2D Dirac fermion system can be topologically nontrivial, and a quantum anomalous Hall state may arise under the simultaneous presence of strong electron correlation.[8]

Experimentally, the most practical method of generating a long-period 2D potential is through the construction of heterostructures, where moiré superlattices with different periods can be realized by controlling the twist angles between two materials. In the case of TIs, the epitaxial growth of films with multi-domain structures on atomically smooth substrates produces regions exhibiting moiré superlattices of varying periods.[9–15] However, this approach only induces moiré potentials that act directly on the bottom surface states. Considering that the epitaxial growth of heterostructures on the top surface is considerably more challenging than that on the bottom surface, the influence of the bottom moiré potential on the top surface states becomes a crucial question, particularly when the top and bottom surface states are decoupled.

Here, we report the growth of Sb_2Te_3 and Bi_2Te_3 epitaxial films on atomically smooth $SrTiO_3$ (STO) (111) substrates. Moiré patterns are observed between the film and the substrate. *In-situ* scanning tunneling spectroscopy (STS) was performed on the top surface of 3- and 4-QL regions of the Sb_2Te_3 film with different moiré periods (a_M). Spatially resolved STS reveals a periodic potential modulation of about 21 meV in the bulk-like bands in regions with $a_M \sim 16$ nm. In contrast, such potential variation is nearly indiscernible in the top surface states, as shown by spatially dependent STS of surface states measured at both 0 T and 14 T. Consequently, no mini-band formation occurs in the surface-state structure, as confirmed by field-dependent Landau-level spectroscopy and simulations. These results indicate distinct modulation effects of external potential variations on bulk and top surface states, highlighting the strongly reduced influence of the bottom moiré potential on the top surface states.

2. Presence of moiré patterns in the 1-QL Sb_2Te_3 /STO system

Few-QL Sb_2Te_3 and Bi_2Te_3 thin films were epitaxially grown on reconstructed STO (111) ($\sqrt{13} \times \sqrt{13}$) (RT13) substrates and investigated using a combined molecular beam

[†]These authors contribute equally to this work.

[‡]Corresponding author. E-mail: zhangjun@ee.ecnu.edu.cn

[§]Corresponding author. E-mail: ypjiang@clpm.ecnu.edu.cn

© 2025 Chinese Physical Society and IOP Publishing Ltd. All rights, including for text and data mining, AI training, and similar technologies, are reserved.

epitaxy (MBE) and low-temperature scanning tunneling microscopy (STM) system. Figures 1(a)–1(f) show the contrasting behaviors of 1-QL Sb_2Te_3 and Bi_2Te_3 films on the substrates. In Sb_2Te_3 films, multi-domain structures with different moiré patterns emerge. Figure 1(a) presents the STM morphology of a $\sim$ 1.2 QL film, where multi-domain structures and moiré patterns are more clearly observed in the derivative image (Fig. 1(b)).

Moiré patterns between the substrate and the first QL are also present in thicker films, as shown in Fig. 1(c) and its derivative image (Fig. 1(d)). In such few-QL topological insulator (TI) films, careful identification is required to distinguish patterns originating from the TI-substrate interface. It should be noted that moiré patterns can also form between different QLs, since the growth dynamics for thicker films may differ from those of the first QL.[16]

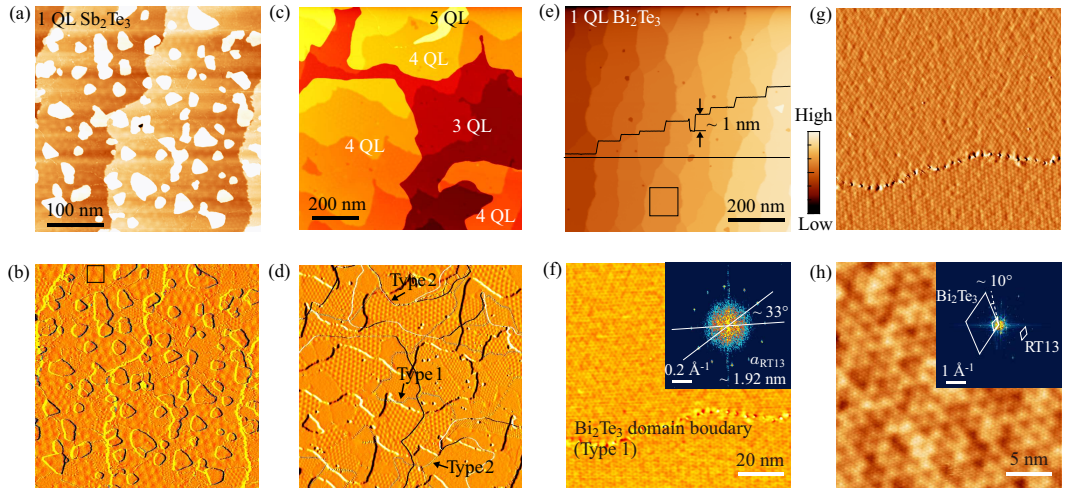


Fig. 1. The a-few-QL Sb_2Te_3 and Bi_2Te_3 films grown on the STO (111) ($\sqrt{13} \times \sqrt{13}$) substrate. (a), (b) The STM and derivative image (3 V, 10 pA) of the 1-QL Sb_2Te_3 film, respectively. The white-colored features in (a) are the second QL. (c), (d) The STM and derivative image (3 V, 10 pA) of the Sb_2Te_3 film composed of 3-, 4-, and 5-QL regions. (e) The STM image (3 V, 10 pA) of the 1-QL Bi_2Te_3 film. The height profile shows the thickness of Bi_2Te_3 as well as the steps of the substrate. (f) The STM image (1 V, 100 pA) of the squared region in (e). The inset is the fast-Fourier transformed (FFT) image. (g) The derivative of (f). (h) The atomically resolved image of 1-QL Bi_2Te_3. The inset is the FFT image. All the STM data were taken at 4.2 K. The STS were taken by measuring the dI/dV signal while sweeping the bias voltage with a 3-mV modulation and keeping feed-back off.

Unlike 1-QL Sb_2Te_3, the 1-QL Bi_2Te_3 film shows no moiré pattern. The large-scale STM image (Fig. 1(e)) reveals a uniform 1-QL Bi_2Te_3 film, whose morphology follows the step structure of the substrate. The thickness is 1 nm, as indicated by the height profile (inset). Figure 1(f) shows the magnified image of the squared region in Fig. 1(e), displaying two superlattices with identical periods ($\sim$ 1.92 nm) but rotated by $\sim$ 33° (Fig. 1(f) and inset FFT image). This period corresponds to the RT13-reconstructed STO (111) surface.[17] In addition, the 1-QL Bi_2Te_3 film exhibits only domain boundaries with much smaller mismatch angles (type 1), as illustrated in the derivative image (Fig. 1(g), dotted defect arrangement along the boundary).[18] Thus, the Bi_2Te_3 domains are nearly aligned in the same direction. An atomically resolved image (Fig. 1(h) and inset FFT image) shows the Bi_2Te_3 and RT13 lattices with a twist angle of $\sim$ 10°, in which case the moiré pattern is too weak to be detected by STM.

In contrast, most domain boundaries in 1-QL Sb_2Te_3 exhibit relatively large rotation angles (type 2), consistent with our previous report.[18] This is corroborated by the distinct RHEED patterns of 1-QL Bi_2Te_3 and 1-QL Sb_2Te_3 (supplementary Fig. S1), which reveal nearly consistent alignment of domains in the former and multiple domain orientations in the latter. Consequently, the relatively random domain orientations in Sb_2Te_3 give rise to a variety of twist angles between Sb_2Te_3 and STO, enabling the emergence of moiré patterns at specific twist angles.

In this study, only the moiré patterns originating from the TI-substrate interface are considered. To unambiguously identify such patterns, high-resolution STM images were obtained, as shown in Figs. 2(a) and 2(b), with moiré periods of $\sim$ 20 nm and $\sim$ 6 nm, respectively. On 1-QL Sb_2Te_3, which has a band gap of $\sim$ 0.7 eV, atomic resolution is difficult to achieve; the 1-QL image only reveals the RT13 lattice and the moiré pattern. In contrast, the 3-QL film shows the TI lattice rather than that of RT13. These observed patterns can be accurately reproduced by simulations of twisted structures between the TI and RT13 lattices, as shown in Figs. 2(c) and 2(d), with twist angles consistent with experimental measurements. The simulated patterns appear relatively weak, which is reasonable due to the substantial mismatch between the Sb_2Te_3 lattice constant and that of the RT13-reconstructed STO substrate. Figures 2(e) and 2(f) present top-view lattice models of the TI and RT13, where only Ti and O atoms of the RT13 lattice are displayed.

3. Unchanged top-surface-state dispersion in 3-QL films with different moiré patterns

Figures 2(g)–2(i) display STM images of 3-QL films showing moiré patterns with different periods (13.6 nm, 6 nm, and none) along with the corresponding field-dependent STS spectra (bottom). Field-dependent Landau levels (LLs) appear in these spectra, from which the surface-state dispersion can be extracted. The STS of these 3-QL films on STO are comparable to those measured for films grown on graphene substrates. The observed gapped features in the spectra arise from hybridization between the top and bottom surface states.[19]

We simulated the field-dependent LLs in 3-QL Sb_2Te_3 films using a gapped surface-state Hamiltonian that includes a coupling term Δ between the top and bottom surface $H = E_D + \hbar v_F(k_y\sigma_x - k_x\sigma_y) + (\Delta + ak^2)\tau_x$.[20] Here E_D, v_F, $\boldsymbol{k}$, $\boldsymbol{\sigma}$, $\boldsymbol{\tau}$ are the Dirac point energy, Fermi velocity, momentum after magnetic Peierls substitution in a perpendicular magnetic field B_z, the spin Pauli matrix, and the Pauli matrix corresponding to the surface index degree of freedom, respectively. The parabolic term accounts for the difference in Fermi velocities between the upper and lower surface-state branches. The eigenstates of this Hamiltonian, i.e., the LLs, can be derived analytically as $E_0 = E_D \pm \left|\Delta - \frac{\alpha}{2}\right|$ and $(E_N - E_D)^2 = \omega_N^2 + (\frac{\alpha}{2})^2 + (\Delta - \alpha N)^2 \pm |\alpha(\Delta - \alpha N)|$ $(N = 1, 2, 3, \ldots)$, where $\alpha = -2eB_z/\hbar$, $\omega_N = v_F\sqrt{2e\hbar B_z N}$. The simulated field-dependent LLs are plotted alongside the experimental data in the lower panel of Fig. 2(i), where the LL indices are labelled. The fitting parameters $E_D = -119$ meV, $v_F = 4.5 \times 10^5$ m/s, $\Delta = 76$ meV, $a = 100$ meV·nm^2. The Fermi velocity agrees with the experimental value measured on the 4-QL film.[19] The nearly perfect agreement between simulation and experimental results supports the absence of mini-band formation in the top surface states.

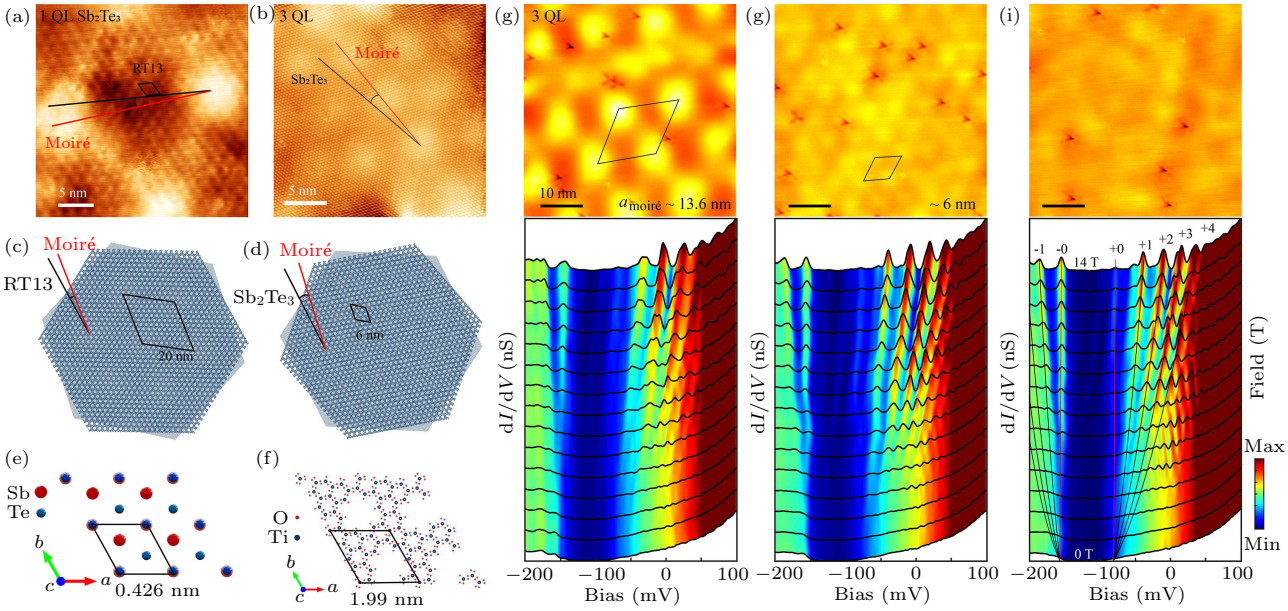


Fig. 2. The simulation of moiré patterns and the surface states on 3-QL Sb_2Te_3 with moiré patterns. (a) The STM image (−2 V, 50 pA) of 1-QL Sb_2Te_3. (b) The STM image (100 mV, 50 pA) of 3-QL Sb_2Te_3. (c), (d) Simulation of the moiré patterns shown in (a) and (b) with periods of about 20 nm and 6 nm, respectively. (e), (f) The surface unit cells of Sb_2Te_3 and STO (111) with reconstruction. (g)–(i) The STM morphologies (top) (1 V, 50 pA) of 3-QL Sb_2Te_3 films with and without moiré patterns and the corresponding field-dependent surface-state LLs.

4. Different effects of moiré patterns on bulk and surface states

The absence of mini-band formation in the top surface states in the presence of moiré patterns is attributed to the significantly reduced moiré potential sensed by the top surface. Figures 3(a) and 3(b) show spatially resolved STS on the 3-QL film with a moiré period of $\sim$ 16 nm, taken along the line indicated in the inset of Fig. 3(d). Spectral features measured in two different energy ranges correspond to bulk-like and surface-like states, respectively. In 3-QL Sb_2Te_3 films, the top and bottom surface states overlap and hybridize. In this ultrathin case, the terms "surface" and "bulk states" refer to whether or not the states exhibit significant spatial dependence along the surface normal direction. STS acquired at relatively large tip-sample distances (0.6 V, 300 pA) display only bulk-like states (Figs. 3(a) and 3(d)), due to the much weaker surface-state density of states compared with bulk-like bands. By reducing the tip–sample distance (0.15 V, 300 pA) and probing within the energy window corresponding to the bulk-like gap, the surface states (SS) can be resolved (Figs. 3(b) and 3(e)).[19]

Potential variations appear in both bulk and surface bands, as indicated by shifts in the bulk valence band (BVB) edge (Figs. 3(a) and 3(d)) and the SS valence band edge (Figs. 3(b) and 3(e)), located around −300 meV and

−100 meV, respectively. For surface states, a parabolic-like potential profile with a depth of ∼ 31 meV is evident from the spatial variation of the $N = -0$ and -1 LLs in spectra taken at 14 T (Fig. 3(c)). For bulk states, in addition to the parabolic variation (dashed curve), a periodic potential modulation of ∼ 21 meV consistent with the moiré pattern is observed. In contrast, such periodic modulation is nearly absent in the surface-state spectra (Fig. 3(c)).

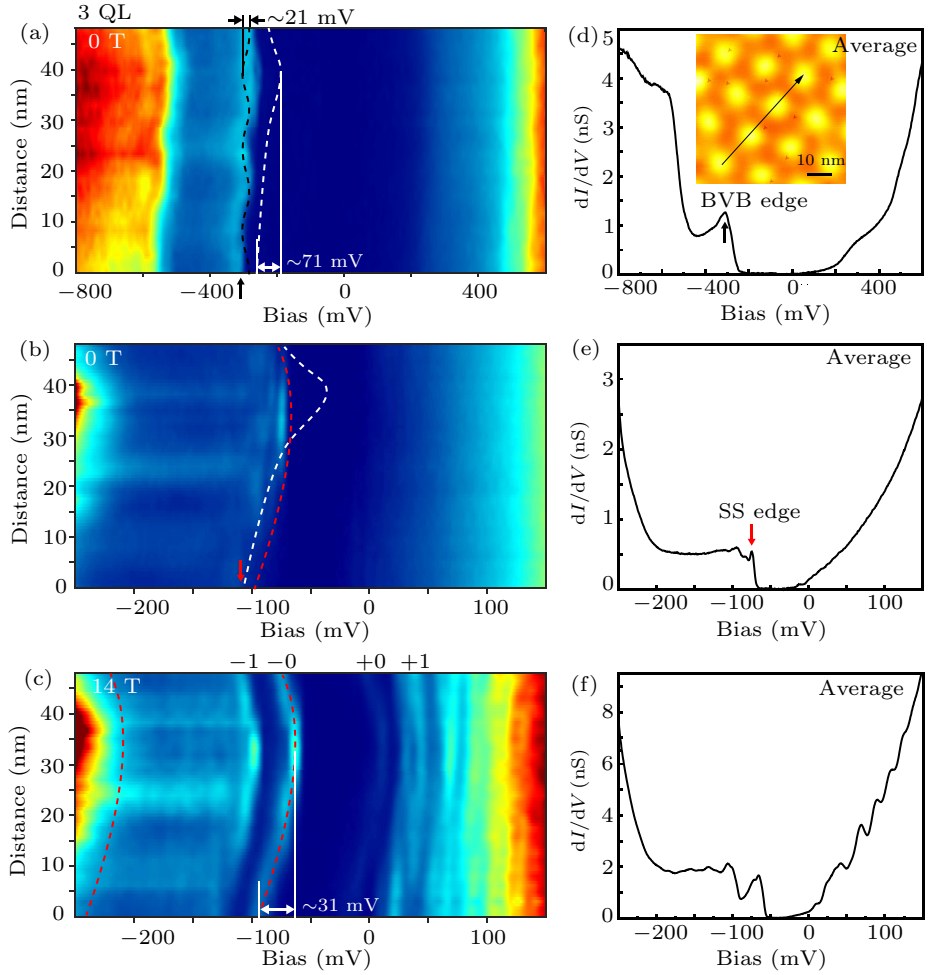


Fig. 3. The effect of moiré patterns on the 3-QL Sb_2Te_3 films. (a)–(c) The dI/dV spectra along the line (inset of (d)) in a larger energy range as well as those in a smaller energy range at 0 T and 14 T, respectively. The periodic black-dashed curve and the white-dashed one are two components that fit the potential profile (the valence band edge as indicated by the arrow) in the bulk states. The red dashed lines in (b) and (c) denote the potential variations in the surface states as indicated by the 0th LL in (c). (d)–(f) The corresponding averaged spectra for (a)–(c). The STM images of moiré patterns in Figs. 3 and 4 are taken at the tunneling condition (1 V, 50 pA).

The parabolic variations in bulk and surface states differ (two dashed curves in Fig. 3(b)), likely due to intrinsic defects distributed across the film thickness, which affect bulk and top surface states differently. In the lower surface-state branch, periodic variation in spectral magnitude is observed (see also Fig. 4(e)), which may originate from spatially dependent tunneling gaps caused by bulk-state contributions to the tunneling current during STS measurements. Figures 3(d)–3(f) show the corresponding averaged spectra.

In 4-QL films, coupling between the top and bottom surfaces is minimized.[19] Spatially resolved STS was performed on 4-QL regions with different moiré periods. The STM images (insets of Figs. 4(b) and 4(f)) show moiré periods of ∼ 10 nm and ∼ 20 nm, respectively. Weak peak-like features in spectra measured at 0 T (arrowed in Figs. 4(a) and 4(e)) are most likely trapped states due to potential variations. These variations lead to spatially dependent splitting of LLs, particularly the 0th LLs (Figs. 4(c) and 4(g)). The potential variation in top surface states is seen in spectra taken at 14 T (Figs. 4(c) and 4(g)). For the $N = +1$ LL, almost no periodic potential variation is found in the $a_M = 10$ nm region. In the larger-period region, the variation does not align with the moiré pattern, suggesting it arises from random defect potentials.

The only difference between these two cases is that periodic variation in spectral magnitude (below the Dirac point) appears in the larger-period case, similar to that observed in 3-QL films. This phenomenon is attributed to bulk-state potential variations reflecting the periodic moiré potential experienced by the film. Thus, moiré patterns with larger periods exert stronger periodic potentials on TI films, primarily affecting bulk states. Moreover, the 'V'-shaped spectra at 0 T and the LL series at 14 T (averaged STS in Figs. 4(b), 4(d), 4(f), 4(h)) indicate nearly decoupled top and bottom surface states, similar to films grown on graphene.[19]

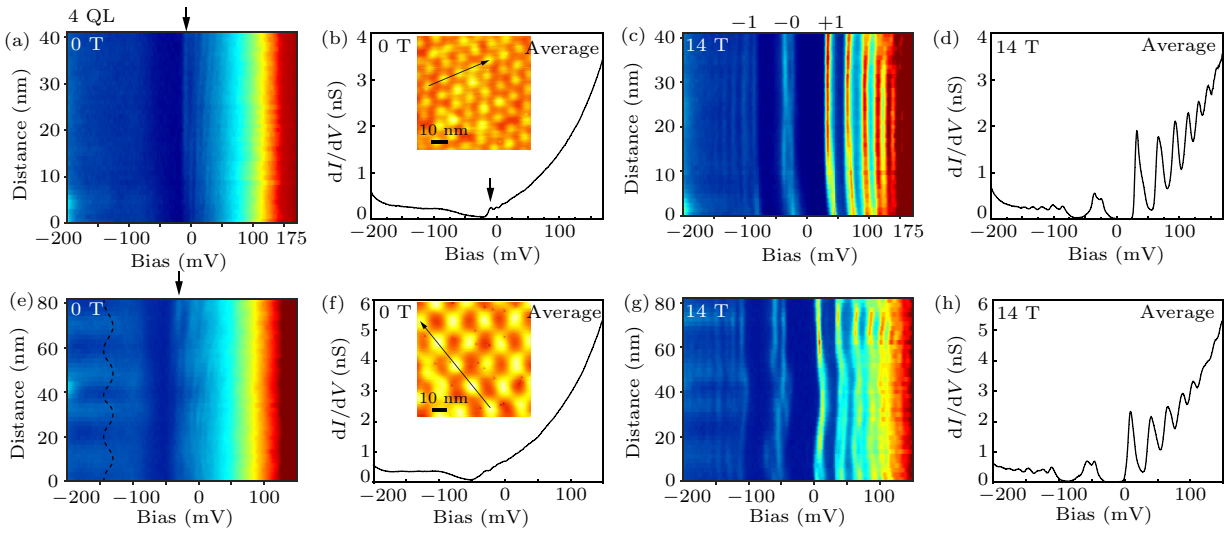


Fig. 4. The effect of moiré patterns on the 4-QL Sb_2Te_3 films. (a) and (c) The dI/dV spectra along the line (inset of (b)) at 0 T and 14 T, respectively. (b) and (d) The corresponding averaged spectra for (a) and (c). (e)–(h) The data along the line (inset of (f)) with a larger moiré period. The short arrows indicate the trapped states. The dashed curve in (e) indicates the periodic magnitude variations below the Dirac point.

5. Discussion

Our experiments demonstrate the formation of moiré patterns at the interface between Sb_2Te_3 thin films and reconstructed STO (111) substrates. We examined the impact of these moiré patterns on bulk and top surface states in 3- and 4-QL Sb_2Te_3 films. Periodic potential variations of ~ 21 meV are observed in bulk states in regions with a moiré period of ~ 16 nm, with larger moiré periods producing stronger potential magnitudes. By contrast, the top surface states sense only minimal moiré potential, preventing mini flat-band formation in 3- and 4-QL films. This conclusion is supported by field-dependent LL spectra, where the surface-state dispersion in 3-QL films matches that of films grown on graphene and is well described by a gapped two-surface model including a coupling term.

Although band-folding may occur in the bottom surface states under a moiré potential of ~ 21 meV, it cannot be probed by surface-sensitive techniques. In simulating LL states of the 3-QL film, a two-surface model with a coupling mass term of ~ 60 meV between top and bottom Dirac states was adopted. If bottom surface states undergo band-structure downfolding, the top surface states could be indirectly affected through coupling. However, mini-band formation is highly dependent on the potential strength.[3] The band-structure modifications in the bottom surface states under a ~ 21 meV moiré potential are likely weak, with possible satellite Dirac cones located away from the original one. Furthermore, top–bottom surface coupling primarily affects states near the original Dirac cone, further suppressing changes in the top surface states.[21]

This study clarifies the distinct roles played by moiré patterns at the TI–substrate interface on bulk states and top surface states in 3D topological insulators.

Acknowledgements

We acknowledge the supporting from the National Key R&D Program of China (Grant No. 2022YFA1403102) and the National Natural Science Foundation of China (Grant Nos. 12474478, 92065102, and 12574094).

References

[1] Miao W, Rashidi A and Dai X 2025 *Phys. Rev. B* **111** 045113
[2] Guerci D, Wang J, Pixley J H and Cano J 2022 *Phys. Rev. B* **106** 245417
[3] Dunbrack A and Cano J 2022 *Phys. Rev. B* **106** 075142
[4] Cano J, Fang S, Pixley J H and Wilson J H 2021 *Phys. Rev. B* **103** 155157
[5] Wang T, Yuan N F Q and Fu L 2021 *Phys. Rev. X* **11** 021024
[6] Suri N, Wang C, Hunt B M and Xiao D 2023 *Phys. Rev. B* **108** 155409
[7] Ghorashi S A A, Dunbrack A, Abouelkomsan A, Sun J, Du X and Cano J 2023 *Phys. Rev. Lett.* **130** 196201
[8] Yang K, Xu Z, Feng Y, Schindler F, Xu Y, Bi Z, Bernevig B A, Tang P and Liu C X 2024 *Nat. Commun.* **15** 2670
[9] Reifsnyder Hickey D, *et al.* 2020 *Phys. Rev. Mater.* **4** 011201
[10] Liu B, Wagner T, Enzner S, Eck P, Kamp M, Sangiovanni G and Claessen R 2023 *Nano Lett.* **23** 3189
[11] Schouteden K, Li Z, Chen T, Song F, Partoens B, Van Haesendonck C and Park K 2016 *Sci. Rep.* **6** 20278
[12] Nakamura T, *et al.* 2024 *Commun. Mater.* **5** 167
[13] Yin Y, *et al.* 2022 *Nano Res.* **15** 1115
[14] Salvato M, *et al.* 2022 *ACS Nano* **16** 13860
[15] Song C L, *et al.* 2010 *Appl. Phys. Lett.* **97** 143118
[16] Zhou C, Song D, Jiang Y and Zhang J 2021 *Chin. Phys. Lett.* **38** 057307
[17] Andersen T K, Wang S, Castell M R, Fong D D and Marks L D 2018 *Surf. Sci.* **675** 36
[18] Zhang J, Cheng J, Ji S and Jiang Y P 2021 *Chin. Phys. Lett.* **38** 077301
[19] Jiang Y, *et al.* 2012 *Phys. Rev. Lett.* **108** 016401
[20] Zhang S F, Jiang H, Xie X C and Sun Q F 2014 *Phys. Rev. B* **89** 155419
[21] Huang H, Chen M, Song D, Zhang J and Jiang Y P 2024 *Phys. Rev. B* **109** 115414